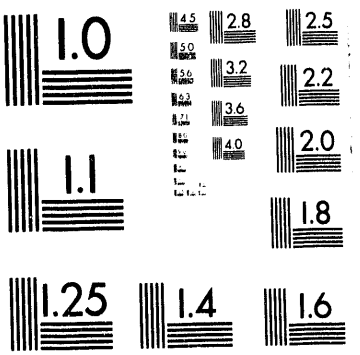
1.0
1.1
1.25
1.4
1.6
1.8
2.0
2.2
2.5
2.8
3.2
3.6
4.0
4.5
5.0
5.6

1 of 1

WSRC-RP-93-997
Task SRT-WAG-93-8001

CPT
Chemical Process
Technology Department

Keywords:
Waste Tanks
Deflagration
Pressure
Combustion
Flame
Radiative
Heat Transfer

Retention - Permanent

POTENTIAL FOR A SOLIDS FIRE DURING AN ITP WASTE TANK DEFLAGRATION AND THE IMPACT ON GAS PRESSURE (U)

By

J. K. Thomas

ISSUED: July 1993

Derivative Classifier

SRTC SAVANNAH RIVER TECHNOLOGY CENTER, AIKEN, SC 29808
Westinghouse Savannah River Company
Prepared for the U. S. Department of Energy under Contract DE-AC09-89SR18035

PROJECT: In-Tank Processing Facility Safety Analysis Support Services

DOCUMENT: WSRC-RP-93-997

TITLE: Potential for a Solids Fire During an ITP Waste Tank Deflagration and the Impact on Gas Pressure (U)

TASK: SRT-WAG-93-8001

APPROVALS

S. J. Hensel — **DATE:** 8-30-93

S. J. Hensel, Technical Reviewer
Scientific Computations Section

Darrel D. Walker — **DATE:** 8/23/93

D. D. Walker, Technical Reviewer
Interim Waste Technology Section

J D Menna — **DATE:** 9/23/93

J. D. Menna, Manager
DWPF & Liquid Waste Analysis Group

M. L. Cowen — **DATE:** 9/23/93

M. L. Cowen, Manager
Nuclear Process Safety Research Section

R. A. Scaggs — **DATE:** 8/30/93

R. A. Scaggs, Customer Review
WM&ER Division

E. J. Majzlik — **DATE:** 9/8/93

E. J. Majzlik, Program Manager
Materials Technology Section

EXECUTIVE SUMMARY

During the In-Tank Precipitation (ITP) process, solid deposits may form at the water-line on internal waste tank surfaces. These solids may be combustible due to the presence of tetraphenylborate compounds and hence there is a potential that a waste tank deflagration could ignite a solids fire. The work described in this report evaluates the potential for a waste tank deflagration to ignite a solids fire and the subsequent effect on gas pressure.

Thermal analyses were performed using a one-dimensional conduction model, radiative heat flux values calculated with the Deflagration Pressure Analysis Code (DPAC), and effective deposit properties calculated from the component properties. It was shown that a solids fire could only be ignited by a waste tank deflagration for a limited range of cases. For the best-estimate mixtures, a solids fire could not be ignited prior to the time the peak gas pressure is reached and would not increase the peak pressure. For the upper-bound mixtures, the thickness of the solid layer which could be ignited is insufficient to increase the energy released by the deflagration by a significant amount. It was also shown that these conclusions are relatively insensitive to uncertainties related to deposit composition. Thus, the contribution from a solids fire to the gas pressure resulting from a waste tank deflagration may be neglected.

TABLE OF CONTENTS

LIST OF TABLES

LIST OF FIGURES

1.0 INTRODUCTION

During the In-Tank Precipitation (ITP) process, solids will be deposited near the water-line on internal waste tank surfaces (primary liner and cooling coil tubes) from the liquid waste slurry. These solids may be combustible due to the presence of tetraphenylborate compounds and hence there is a potential that a waste tank deflagration could ignite a solids fire. The work described in this report evaluates the potential for a waste tank deflagration to ignite a solids fire and the subsequent effect on gas pressure.

The pressures resulting from deflagrations of hydrogen-benzene (H_2-C_6H_6) mixtures in an ITP waste tank were evaluated by Thomas and Hensel (1993a); however, they did not consider the potential contribution to gas pressure from a solids fire. Walker (1990) has evaluated the contribution to the gas pressure developed during a deflagration as a result of a solids fire; however, Walker assumed that all solids present would burn, whereas the work reported here demonstrates that this will not occur and considers the pressure rise due to that portion of the solid which could burn.

Section 2 presents a characterization of the deposits expected to be formed in ITP waste tanks and present during a deflagration. An analysis of the thermal response of such deposits to an ITP waste tank deflagration is presented in Section 3; the thermal analysis includes an uncertainty evaluation. Section 4 examines the effect of a solids fire on gas pressure and Section 5 presents the conclusions of this work.

2.0 SOLID DEPOSIT CHARACTERIZATION

2.1 Composition

The deposits formed in the ITP tanks will be composed of soluble solids, insoluble solids, and water. The soluble solids will be composed primarily of sodium nitrate ($NaNO_3$), but will also include sodium nitrite ($NaNO_2$), sodium hydroxide (NaOH), and sodium sulfate (Na_2SO_4) in lesser amounts (Walker and Schmitz 1984, Walker 1989). The insoluble solid component will be almost entirely potassium tetraphenylborate (KTPB, $KBC_{24}H_{20}$), but will also contain small amounts of cesium and sodium tetraphenylborate salts (CsTPB and NaTPB) and sodium titanate ($NaTi_2O_5H$). The ratio of soluble to insoluble solids depends upon the conditions under which the deposit is formed, primarily upon the concentration of soluble salts in the slurry. The deposits formed from unwashed slurries have a high mass fraction of soluble solids, while those formed from washed slurries have a higher insoluble mass fraction. Deposits formed from unwashed slurries ignite and support combustion more readily than those formed from washed slurries (Walker 1993) and hence are of more interest in this evaluation. For these reasons, it was assumed that the solid fraction of a deposit would be comprised entirely of $NaNO_3$; the thermal properties of the other solid components are not greatly different than those for $NaNO_3$ and the sensitivity of the results to this assumption is discussed in Section 3.6.

Walker (1989) reports that the deposits formed on coupons dipped repeatedly into simulated slurry had a density of 0.4 gm/cm^3 after drying at 23°C in an atmosphere with a relative humidity of 60%. The measured water content of the deposits was 18% by weight. Both deposit density and water content were approximately the same for a range of soluble to insoluble solid mass fraction ratios. The liquid and solid volume fractions can be calculated as:

$$v_{f,l} = \frac{\rho_d \, m_{f,l}}{\rho_l} \tag{1}$$

$$v_{f,s} = \frac{\rho_d \, m_{f,s}}{\rho_s} = \frac{\rho_d \, (1 - m_{f,l})}{\rho_s} \tag{2}$$

where: v_f = Volume fraction,
m_f = Mass fraction, and
ρ = Density

The 's' and 'l' subscripts refer to the solid and liquid components of the deposit, respectively, and the 'd' subscript refers to the deposit as a whole. The liquid (water)

volume fraction corresponding to a 18% liquid mass fraction, a 0.4 gm/cm^3 deposit density, and a 1.0 gm/cm^3 liquid density is 7.2% ($m_{f,l}$ = 0.072). Taking a solid density of 2.3 gm/cm^3 [e.g. $NaNO_3$ (Weast and Astle 1982)] and a mass fraction of 82% with eqn.(2) gives a solid volume fraction of 14%. Thus, the dried coupon deposits had a void (air) volume fraction of approximately 79% (100 - 7 - 14 = 79). If this void space were filled with water, the total liquid volume fraction would be 86% (79 + 7 = 86); the corresponding liquid mass fraction can be calculated as:

$$m_{f,l} = \frac{\rho_l v_{f,l}}{\rho_l v_{f,l} + \rho_s v_{f,s}} \qquad (3)$$

which gives a liquid mass fraction of 73% for the volume fractions and densities given above. This value agrees with the 72 to 74% liquid mass fractions reported by Walker (1989) for deposits formed from unwashed slurries and subjected to high humidity conditions (≈ 90% R.H.) at 23°C. This is also in good agreement with the 77.5% liquid mass fraction measured for a deposit taken from a tank (TNX Tank W2) holding simulated washed precipitate a few days after the tank had been drained (Walker 1989).

Since the relative humidity inside a waste tank a short time after the nitrogen purge is lost would be at least 90% (Morin 1993) and the vapor temperature would be well above 23°C, the deposit liquid volume fraction would be approximately 86% [e.g. all deposit volume occupied by either liquid (86%) or solid (14%)]. The corresponding mass fractions for liquid density of 0.96 gm/cm^3 (e.g. H_2O at 100°C) and a solid density of 2.3 gm/cm^3 are 28% (solid) and 72% (liquid). These mass and volume fractions were used in Section 3.3 to develop the solid deposit thermal properties. Note that if the deposit were to be heated as the result of a waste tank deflagration, then the liquid phase component would boil off if the deposit temperature exceeded 100°C (ignoring the slight boiling point increase due to dissolved salts and elevated pressure) and the remaining deposit would have a very high porosity.

2.2 Deposit Flammability Characteristics

Differential Thermal Analysis (DTA) tests run in air with dried deposits formed from a range of slurry compositions and with reagent grade sodium tetraphenylborate (NaTPB) showed that the deposit temperature must exceed at least 300°C prior to the onset of any exothermic reactions (Walker 1989). Autoignition temperature (AIT) and autooxidation temperature (AOT) tests on dried slurry deposits also confirmed that the deposit temperature must exceed approximately 300°C prior to the onset of exothermic reactions

or ignition. On the basis of these data, it is assumed that the surface of a deposit inside the waste tank would have to be heated to at least 300°C before ignition would be possible. Note that the experimental data reported in Walker (1989) from tests conducted at DuPont's Engineering Test Center demonstrated that some deposits will not ignite even under a propane torch flame. The assumption that a 300°C surface temperature would lead to ignition is therefore conservative.

Tests with dried deposits ignited by direct contact with a hot wire demonstrated that the minimum oxygen concentration (MOC) for propagation of a solids fire is at least 12% (Walker 1989). A solids fire may be ignited at an oxygen concentration of less than 12%, but it will not propagate and will be rapidly self-extinguished once the ignition source is removed.

2.3 Combustion Energy Balance

Walker (1990) reports that the maximum energy release from a solids fire would occur if the combustion was described by the following reaction:

$$24NaNO_3 + NaBC_{24}H_{20} \rightarrow 12N_2 + 10H_2O + 12Na_2CO_3 + 12CO_2 \quad (4)$$

Walker gives a heat of combustion for this reaction of 2822 kcal per mole of sodium tetraphenylborate ($NaBC_{24}H_{20}$). This reaction provides a bounding energy release value, but is not intended to actually represent the process by which the deposits combust. As discussed above, the deposit requires an atmosphere with a minimum oxygen concentration for sustained combustion once the heat source is removed so that little if any oxygen is actually provided by the sodium nitrate.

Using the heat of combustion and the stoichiometric ratios for eqn.(4) gives a heat of combustion of 1.19 kcal per gram of solid, or 0.33 kcal per gram of deposit (solid mass fraction = 0.28). Thermal radiation would not penetrate into the solid and would only be capable of directly heating the surface. Assuming that this reaction can be initiated at the deposit surface due to radiant energy deposition, then for the reaction to be self-sustaining (so as to allow the bulk of the deposit to combust), the energy liberated by combustion must be equal to or greater than the energy required to heat the deposit to the ignition temperature. As discussed above, the minimum temperature required to initiate sustained combustion in a dry deposit is at least 300°C. The energies required to raise the temperature of water from 40 to 100°C and then to boil it are 60 and 539 cal/g (per gram of H_2O) and the energy required to raise the temperature of sodium nitrate from 40 to

300°C is 88 cal/g (per gram of $NaNO_3$). This gives a total energy requirement of 0.46 kcal per gram of deposit for liquid and solid mass fractions of 0.72 and 0.28; note that the energy required to boil off the water dominates (85% of total energy required).

Since 37% more energy is required to heat the deposit up to the minimum ignition temperature than is released by combustion (0.46 vs. 0.33 kcal/g), the reaction cannot be sustained and only a thin outer layer first dried by radiant heating can combust. The difference between the energy released by combustion and that required to heat the deposit to the ignition temperature may be even larger than given above since a maximum energy release and a minimum ignition temperature were employed. Furthermore, most of the energy liberated by solids combustion would actually be carried away by the gas products and would not be available to heat adjacent regions. Thus, if the reaction proceeded it would represent a net energy sink, not an energy source.

2.4 Combustion Rate

Walker (1989) describes a series of combustion tests conducted at DuPont's Engineering Test Center on deposits formed from slurries and subsequently dried at temperatures above 100°C (e.g. so that most of the deposit water content would be driven off). The deposits most representative of those which would be formed due to waste tank liquid level variations were formed by dipping a 6" x 0.5" vertical surface repeatedly into a slurry; the resulting deposit thickness values ranged from 1/8 to 1/4". The time required to consume the deposit once ignited ranged from 1.4 to 5.8 minutes, which gives a maximum volumetric burn rate of 0.11 cm^3/sec [(6")(0.5")(3/16")/(1.4 min.)] and a maximum linear burn rate of 0.18 cm/sec [(6")/(1.4 min.)]. Although these tests are not directly applicable to the case of a thick deposit ignited at the surface and propagating through its thickness, the results suggest that at least 5 to 10 seconds would be required to consume a 1 cm thick deposit assuming that combustion could be sustained (e.g. assuming a partially dried deposit).

3.0 THERMAL ANALYSIS

3.1 Radiative Heat Flux

The radiative heat flux - time profiles employed in this evaluation were calculated using the Deflagration Pressure Analysis Code (DPAC) for Tank 48 at a 1/10 fill level with a hydrogen to benzene mole ratio of 40/60 (the normal condition) and an initial temperature of 40°C (Thomas and Hensel 1993a). The DPAC code is described in Hensel (1993) and the radiative heat transfer model employed by DPAC is presented in Thomas (1993). Tank 48 was selected since it has the smaller vent area of the tanks of interest in the ITP process (Tanks 48 and 49) and hence the gas pressures which would result from a deflagration in Tank 48 would be larger for a given combustible gas concentration. The 1/10 fill level was employed since lower fill levels give higher gas pressure and radiative heat flux values. As discussed in Appendix B, the contribution of convection to the total heat flux incident on a deposit can be neglected.

The radiative heat flux - time histories resulting from deflagrations of two gas mixture classes were considered in this evaluation. The first class is the best-estimate compositions which consider the effects of the initial N_2 purge gas and water vapor in the air; these compositions were calculated by Morin (1993) assuming inleakage of air due to atmospheric exchange mechanisms after a loss of the N_2 purge gas system. Times after loss of ventilation of 3, 12 and 30 days were examined here. The second class is the upper-bound mixtures of combustible gases with air containing no excess N_2. Combustible gas concentrations at the lower flammability limit (LFL), the stoichiometric value, and half way between the LFL and stoichiometric value were considered in this evaluation.

The specific cases employed are listed in Table 1; Table 2 gives the gas compositions for each of these cases. The case numbers, peak pressures, and burn time values given in Table 1 are taken from Thomas and Hensel (1993a). The time to peak pressure values and radiative heat fluxes were taken from the task records for SRTC/NRTSC Task 93-009-1 (Thomas and Hensel 1993b). The radiative heat flux and gas pressure time histories for the best-estimate and upper-bound cases are shown in Figures 1 and 2, respectively; note that the scales employed in Figures 1 and 2 are different. The radiative heat fluxes given in Table 1 are averages over the time to peak pressure and the total burn time.

The radiative heat flux histories shown in Figures 1 and 2 and averages given in Table 1 are for the cooling coil tubes; the values for the inner surfaces of the waste tank are 10 to 15% lower. Furthermore, these heat fluxes are calculated assuming that the tank vapor space is completely filled with hot product gas (the radiative heat rate calculated by DPAC is taken to be these values multiplied by the fraction of the vapor space actually occupied by product gas) and are therefore applicable only to cooling coil tubes located very near the ignition source; lower values would be predicted for all other locations in the tank. It should also be noted that the heat flux values calculated by DPAC do not include the contribution from convection; however, as discussed in Appendix B, this contribution would be small. It is expected that the use of maximum radiative heat flux values more than compensates for neglecting convective heat transfer.

DPAC shuts off venting if the pressure drops below that initially required to open the vents, which is a conservative approach adopted for simplicity (Thomas and Hensel 1993a). Since the ITP tanks have a large amount of vent area and the burn times are relatively long, the calculated gas pressure for most cases increases to that required to open the vents and then remains at approximately this value throughout the burn. A small pressure spike is calculated at the end of the burn due to autoignition of the remaining reactant gas. However, it is expected that: 1) the gas pressure would actually drop off after the vents are opened, and 2) that autoignition would either not occur or that the pressure spike due to autoignition would be small. The drop off in gas pressure after the vents open was demonstrated in a confirmatory waste tank deflagration analysis performed by Allison and Chow (1993). For the purposes of this evaluation, the autoignition pressure spike calculated by DPAC was ignored for cases where venting was turned off and the time to open the vents was taken as the time to the maximum gas pressure. Only for Case 19a (the stoichiometric upper-bound case) is venting not shut off during a portion of the burn and for this case the pressure spike due to autoignition does not exceed the maximum pressure, which occurs earlier in the burn.

3.2 Thermal Model

The transient through-wall temperature profile for a constant heat flux on a wall which is insulated on the opposite side can be expressed as (Carslaw and Jaeger 1959):

$$\Delta T(x,t) = \frac{q_r t}{\rho C_p L} + \left(\frac{q_r L}{k}\right)\left\{\frac{3x^2 - L^2}{6L^2} - \frac{2}{\pi^2}\sum_{n=1}^{\infty}\left[\frac{(-1)^n}{n^2}\exp\left(\frac{-\alpha n^2 \pi^2 t}{L^2}\right)\cos\left(\frac{n\pi x}{L}\right)\right]\right\} \quad (5)$$

where: ΔT = Temperature increase,
x = Distance from insulated surface,
t = Time,
q_r = Heat flux,
ρ = Density,
C_p = Specific heat,
L = Wall thickness,
k = Thermal conductivity, and
α = Thermal diffusivity.

The temperature increase at the surface (x = L) is therefore:

$$\Delta T_s(t) = \frac{q_r t}{\rho C_p L} + \left(\frac{q_r L}{k}\right)\left\{\frac{1}{3} - \frac{2}{\pi^2}\sum_{n=1}^{\infty}\left[\frac{1}{n^2}\exp\left(\frac{-\alpha n^2 \pi^2 t}{L^2}\right)\right]\right\} \quad (6)$$

where: ΔT_s = Surface temperature increase.

Since the deposit has a low thermal conductivity and the transient time is relatively short, the wall thickness (L) should not have a large impact on the surface temperature. In this case, the semiinfinite wall solution should give approximately the same values as those from the finite wall thickness solution. The transient through-wall temperature profile for a constant heat flux on a semiinfinite wall can be expressed as (Carslaw and Jaeger 1959, Incropera and DeWitt 1981):

$$\Delta T(x,t) = \left(\frac{2 q_r}{k}\right)\sqrt{\frac{\alpha t}{\pi}}\exp\left(\frac{-x^2}{4\alpha t}\right) - \left(\frac{q_r x}{k}\right)\mathrm{erfc}\left(\frac{x}{2\sqrt{\alpha t}}\right) \quad (7)$$

In this expression, 'x' is the distance from the surface exposed to the heat flux. The temperature increase at the surface (x = 0) is therefore:

$$\Delta T_s(t) = \left(\frac{2 q_r}{k}\right)\sqrt{\frac{\alpha t}{\pi}} \quad (8)$$

3.3 Thermal Properties

As discussed in Section 2.1, the solid deposit is assumed to be a composite of $NaNO_3$ and water. The effective specific heat of the deposit is the mass average of the component values, as shown below:

$$C_{p,eff} = (m_{f,s})\cdot(C_{p,s}) + (m_{f,l})\cdot(C_{p,l}) \quad (9)$$

where: $C_{p,eff}$ = Effective deposit specific heat,
$m_{f,j}$ = Mass fraction of the jth deposit component, and
$C_{p,j}$ = Specific heat of the jth deposit component.

The effective density is the volume average of the component values, as shown below:

$$\rho_{eff} = (v_{f,s})\cdot(\rho_s) + (v_{f,l})\cdot(\rho_l) \quad (10)$$

where: ρ_{eff} = Effective deposit density,
$v_{f,j}$ = Volume fraction of the jth deposit component, and
ρ_j = Specific heat of the jth deposit component.

The effective thermal conductivity of the deposit is dependent upon the geometric arrangement of the solid and liquid phases. For the purposes of this evaluation, the deposit is assumed to be a square grid of $NaNO_3$, the pores of which are filled with either water or steam. The effective thermal conductivity of a unit cell in the square grid, calculated in Appendix A using the electrical resistance analog approach, can be expressed as:

$$k_{eff} = \frac{k_s\left(\frac{2-x}{1-x}\right) + k_l\left(\frac{1-x}{x}\right)}{x\left(\frac{2-x}{1-x}\right) + \frac{k_l}{k_s}(1-x) + \frac{1}{x}} \quad (11)$$

where: k_{eff} = Effective deposit thermal conductivity,
k_j = Thermal conductivity of the jth deposit component and
x = Fractional width of solid ligament between adjacent liquid cells.

As shown in Appendix A, the ligament thickness to cell width ratio can be expressed as:

$$x = 1 - (v_{f,l})^{1/3} \quad (12)$$

and for a specified water region width (w) the solid ligament thickness is:

$$x = w\left[(v_{f,l})^{-1/3} - 1\right] \quad (13)$$

3.3.1 Below 100°C

No water loss would occur below 100°C so that the liquid volume fraction is taken to be 0.86, as discussed in Section 2.1. The specific heat, thermal conductivity and density of $NaNO_3$ at 100°C are 1.2 J/g/K, 0.57 W/m/K, and 2.3 gm/cm^3 (Touloukian and Buyco 1970, Touloukian et al. 1970, Weast and Astle 1982). The specific heat, thermal conductivity and density of liquid water at 100°C are 4.2 J/g/K, 0.68 W/m/K, and 0.96 gm/cm^3 (Incropera and DeWitt 1981). The mass and volume fractions, effective specific heat, thermal conductivity and density computed using these values with eqns. (9) through (12) are summarized in Table 3. Note that the actual geometric structure of the deposit would have little impact on the calculated effective deposit thermal conductivity since the solid and liquid thermal conductivities are not significantly different.

3.3.2 100 to 300°C (dry)

The deposit would completely dry out above 100°C since the water would boil off. The steam volume fraction is equal to that of the liquid below 100°C (0.86). The heat capacity of the steam may be neglected since it is very small compared to that of the solid. The specific heat of $NaNO_3$ at 300°C is 1.6 J/g/K (Touloukian and Buyco 1970), which gives an average over the 100 to 300°C range of 1.4 J/g/K. The $NaNO_3$ conductivity and density values at 100°C were also used at 300°C. The thermal conductivity of steam at 200°C and 1 atmosphere is 0.032 W/m/K (Incropera and DeWitt 1981); this value increases only slightly with pressure. The mass and volume fractions, effective specific heat, thermal conductivity and density computed using these values with eqns. (9) through (12) are summarized in Table 3. The effective thermal conductivity of the deposit is very low above 100°C due to the large steam volume fraction (an order of magnitude lower than for liquid-filled pores). Note that the effective thermal conductivity would be increased if the initial liquid volume fraction were decreased.

3.3.3 40 to 300°C (wet)

The same values as given above for the 100 to 300°C (dry) case are employed here, with the exception that the effective deposit specific heat is increased to account for the energy required to vaporize the water. This contribution can be calculated as:

$$\Delta C_p = \left(\frac{h_{fg} + \overline{C_p}(100°C - 40°C)}{300°C - 40°C} \right) \left(\frac{m_{f,l}}{m_{f,s}} \right) \qquad (14)$$

where: ΔC_p = Increase in specific heat due to liquid boiling,
h_{fg} = Heat of vaporization of liquid at 100°C,
$\overline{C_p}$ = Average specific heat of liquid between 40 and 100°C,
mf,l = Mass fraction of liquid (prior to boiling), and
mf,s = Mass fraction of solid (prior to boiling).

The ΔC_p expression is expressed on a per unit solid mass basis so that it may be used with the post-dryout mass fractions (e.g. $m_{f,l} = 0$, $m_{f,s} = 1$). The heat of vaporization and average specific heat for water are 2257 J/g and 4.2 J/g/K (Incropera and DeWitt 1981), which gives a ΔC_p of 24.8 J/g/K for the liquid and solid mass fractions given above. Note that the effective deposit thermal conductivity was not increased to account for the presence of water from 40 to 100°C, which is conservative. The effective specific heat would be decreased if the initial liquid volume fraction were decreased.

3.4 Effect of Pore Size on Thermal Response

The size of the pores in the deposit will not exert a strong influence on the deposit thermal response if the material contained in the pores is all in a single phase (e.g. water or steam). However, pore size will exert a strong influence on thermal response as the surface temperature is raised above the boiling point and dryout begins. If the deposit has very small pores, then the small mass of water in the layer of pores nearest the surface would boil rapidly and the surface temperature would increase very quickly due to the low deposit effective thermal conductivity after dryout. Alternatively, if the deposit has large pores, then the mass of water in the first layer of pores will be large and hence dryout of this layer, and the subsequent increase in the surface temperature, would be significantly delayed. Small in this context is relative to the dimensions of the deposit; for a 1 cm thick deposit, pores with a characteristic dimension of 1 mm are large, while pores with a characteristic dimension on the order of 0.1 mm (100 μm) or less are small. A deposit with small pores would resemble a wet piece of charcoal, while a deposit with large pores would more closely resemble a kitchen sponge. Figure 3 shows a schematic of deposits with small and large pores. The thermal analyses presented in Section 3.5 treats deposits with small and large pores separately due to the significant differences in their thermal response if the surface temperature exceeds the boiling point.

3.5 Results

It is assumed that the deposit would not ignite if the deposit surface temperature does not exceed 300°C prior to the end of the burn since the heat flux to the surface would decrease dramatically after the combustion process ceased. If ignition occurred prior to the end of the burn, but after the peak gas pressure from the deflagration had already been reached, then the energy release from the solid would have to be very large and/or occur over a very short time span in order to increase the peak gas pressure. As discussed in Sections 2.3 and 2.4, the energy release from a solids fire would not be large and the rate of release would not be greatly different than that from the deflagration; hence ignition after the peak pressure had been reached would not increase the peak pressure. Only if a solids fire was ignited prior to time the peak pressure from the deflagration is reached could the peak pressure be increased. Furthermore, for all of the best-estimate cases and most of the upper-bound cases, the magnitude and rate of energy release from the deflagration would not be large enough to increase the gas pressure above that required to open the vents so that the small increase in total energy release from a solids fire would not increase the peak gas pressure. Hence, the only real case of concern is if a solids fire could be ignited prior to reaching the peak gas pressure for a deflagration of a near-

stoichiometric mixture of combustible gas with air (e.g. Case 19a). In spite of these conclusions, the analyses of the deposit thermal response to a deflagration were carried out for a range of both best-estimate and upper-bound cases for the sake of completeness.

It was verified that the insulated and semiinfinite wall temperature distribution expressions developed in Section 3.2 give approximately the same values for the range of radiative heat flux, time, property, and deposit thickness values of interest. The semiinfinite solutions [eqns. (7) and (8)] were used to calculate the values reported in this section. The results are summarized in Table 4 and are discussed below.

3.5.1 Small Pore Model

The thermal analysis for the small pore model was performed in 2 steps. First, an analysis was conducted using the 1st set of property data in Table 3, which is valid up to 100°C. If the surface temperature was calculated to exceed 100°C prior to the end of the deflagration, then the surface temperature was recalculated using the 3rd set of property data in Table 3 (which ignores the thermal conductivity of the water but smears its heat of vaporization over the range from 40 to 300°C); note that for a given time this smearing technique will underpredict temperatures below 100°C and overpredict temperatures above 100°C, however this approximation is acceptable since only the time at which the surface reaches 300°C is of interest.

The deposit surface temperature would be maintained below 100°C throughout a deflagration of a best-estimate mixture occurring up to at least 3 days after loss of the purge gas system (Case BE 7). The surface temperature would exceed 100°C for deflagrations ignited after longer periods. For example, 12 days after the loss of the purge gas system (Case BE 9), the surface temperature would reach 100°C at 5 seconds after ignition, approximately the same time the peak pressure would be reached. For all the upper-bound mixtures, the surface temperature would exceed 100°C before the peak gas pressure was reached.

The deposit surface temperature would not exceed 300°C prior to reaching the peak pressure for deflagrations of best-estimate gas compositions; however, the surface could exceed 300°C prior to the end of the burn in deflagrations which occur long after the purge gas system has been lost. For example, 30 days after the loss of the purge gas system (Case BE 12), the surface temperature would reach 300°C 12 seconds after ignition, which is 7 seconds after the peak pressure would be reached but 5 seconds

before the end of the burn. For all the upper-bound mixtures, the surface temperature would exceed 300°C before the peak gas pressure was reached.

As discussed above, the surface temperature is calculated to exceed 300°C prior to the end of the burn for deflagrations of some of the best-estimate and all of the upper-bound gas compositions. However, since the thermal conductivity of the dry deposit is very low, the thickness of the layer above 300°C would be very small. The depth to which the 300°C limit would be exceeded was calculated using eqn.(7), the 3rd property set in Table 3, and the total burn time - radiative heat flux sets for the bounding best-estimate and upper-bound deflagrations (Cases BE 12 and UB 19a). The calculated temperature profiles are approximate since: (1) the thermal conductivity of the region of the deposit which would still be below 100°C is underpredicted by an order of magnitude so that heat flow away from the surface is underpredicted, (2) the radiative heat fluxes calculated by DPAC assume that the surface temperature is sufficiently low that thermal radiation emissions from the surface may be neglected (e.g. $T_{gas}^4 >> T_s^4$) so that the net radiative heat flux to the surface would be decreased relative to the values employed here (this would only significantly impact the upper-bound case), and (3) the effective specific heat used in the analysis includes a very large contribution from the water heat of vaporization smeared over 40 to 300°C, so that surface temperatures above 300°C are underpredicted (this would only significantly impact the upper-bound case). The calculated temperature profiles are shown for several times up to and including the total burn time in Figures 4 (Case BE 12) and 5 (Case UB 19a). For a radiative heat flux of 5.6 W/cm^2 (Case BE 12), less than 0.1 mm of the deposit would be heated above 300°C within 17 seconds (the burn time for Case BE 12). A radiative heat flux of 34 W/cm^2 (Case UB 19a) would heat less than 0.4 mm of the deposit above 300°C within 7 seconds (the burn time for Case UB 19a). Therefore, although the surface temperature is calculated to exceed 300°C in some cases, the thickness of the layer which would exceed 300°C would be very small (less than 0.4 mm).

3.5.2 Large Pore Model

The thermal analysis for the large pore model was also performed in 2 steps. First, the time to boil off a 1 mm thick layer of water was computed as:

$$t_b = \frac{h_{fg}\,\rho_l\,w}{q_r} \qquad (15)$$

where: t_b = Time to boil water layer,
h_{fg} = Heat of vaporization for water at 100°C (2257 J/g), and

w = Width of water layer.

Next, the time to heat the dry solid from 100 to 300°C was calculate using the 2nd set of property data in Table 3; this neglects the high thermal conductivity of the portion of the solid away from the surface which is still below 100°C, thus decreasing heat transport from the surface and increasing the surface temperature, which is conservative. The time to heat the deposit surface from 40 to 300°C was taken to be the sum of: (1) the time to heat the surface from 40 to 100°C calculated with the small pore model (as discussed previously in Section 3.5.1), (2) the time to boil off the 1 mm thick water layer as described above, and (3) the time to heat the dry solid from 100 to 300°C calculated using the 2nd set of property data in Table 3.

The calculated time to boil the water layer exceeds the burn time for all of the best-estimate and upper-bound cases; the time to boil the water layer is much larger than the burn time for the best-estimate cases. The small contributions to the total time to reach 300°C from the times required to heat the solid up from 40 to 100°C and from 100 to 300°C is expected based on the heat capacity arguments presented in Section 2.3.

Note that even if a surface temperature was calculated to exceed 300°C, this would only imply combustion of the outer solid layer and not of the entire deposit. The remainder of the deposit would still be wet and a 2nd cycle of boiling would have to be completed to gain access to the 2nd solid layer. The solid layer thickness calculated using eqn.(13) with a 1 mm liquid width and a liquid volume fraction of 0.86 is only 0.05 mm. Assuming larger liquid widths would increase the solid volume exposed at dryout, but would linearly increase the time required to boil off the water, while assuming significantly smaller liquid widths would give the same results as the small pore model.

3.6 Uncertainty and Sensitivity Evaluation

As discussed in Section 2.1, the deposits formed in the ITP tanks will be composed of soluble solids, insoluble solids, and water. The deposits most likely to undergo sustained combustion would be those formed from unwashed slurries (Walker 1993), which would have a high mass fraction of soluble solids with sodium nitrate ($NaNO_3$) being the major soluble solid component (Walker and Schmitz 1984, Walker 1989). For this reason, the solid portion of the deposit was assumed to be $NaNO_3$ in developing the effective deposit properties (Section 3.3). The uncertainties due to this assumption dominate all other sources of uncertainty in the evaluation (e.g. heat flux, burn time, deposit geometry). The

uncertainty due to deposit composition is discussed below in 2 parts: (1) that due to the presence of other soluble solids, and (2) that due to the presence of insoluble solids.

The properties of the major soluble solid components should all be similar. For example, the density of $NaNO_3$ is 2.26 gm/cm^3 (Weast and Astle 1982) and the other significant soluble solid components ($NaNO_2$, NaOH and Na_2SO_4) have densities ranging from 2 17 to 2.68 gm/cm^3 (Weast and Astle 1982). Thermal properties were not located for all the soluble components. However, the thermal conductivity of $NaNO_3$ (0.6 W/m/K) is on the low end for a salt; for comparison, the thermal conductivity of NaOH is approximately 0.9 W/m/K (Touloukian et al. 1970). Therefore, it is expected that the results presented in this report would not be significantly impacted by the presence of small quantities of other soluble solid components.

The properties of the deposit could be impacted if the insoluble solid (e.g. KTPB) content were significant, as would be the case for a deposit formed from a washed slurry. The density of KTPB is 1.2 gm/cm^3 (Arnott and Abrahams 1958), which is much lower than that for $NaNO_3$ (2.3 gm/cm^3). Lowering the deposit density by a factor of 2 would increase the solid volume fraction by a factor of 2 [eqn. (2)]. For a given set of solid thermal properties, increasing the solid volume fraction will increase the effective deposit thermal conductivity above the liquid boiling point since the area available for heat transport is increased, and decrease the effective deposit specific heat since less liquid will boil. Thermal property data for solid KTPB was not located in the literature. However, Hovis and McGlynn (1993) report thermal conductivity data for deposits created from a simulated washed slurry with a high solids content (0.4 M Na, 0.2 M NO_3, $\approx$ 12 wt.% insoluble solids [primarily KTPB], and $\approx$ 4 wt.% soluble solids [primarily $NaNO_3$]); this slurry was taken from the Precipitate Hydrolysis Experimental Facility (PHEF) at TNX. Thermal conductivity measurements were made with the deposit immersed in the simulated slurry. Hovis and McGlynn report a thermal conductivity of 0.5 W/m/K ($\pm$ 43%), which is not greatly different than that for $NaNO_3$ (0.57 W/m/K) or the calculated effective deposit value below 100°C (0.66 W/m/K). It is noted that Hovis and McGlynn reported this data as Non-Critical; however, since they are used as confirmatory rather than primary data in this evaluation, the Non-Critical QA status does not preclude their use. On this basis, it is expected that the major uncertainty introduced by the presence of a high KTPB solid mass fraction would be related to the increased solid volume fraction rather than any change in the solid component thermal properties. The sections below present results which illustrate the lack of sensitivity of the thermal

analysis results to an increase in the solid volume fraction by a factor of 2, as might be expected if the solid component of a deposit were primarily KTPB as opposed to primarily $NaNO_3$.

3.6.1 Sensitivity of Property Values [40 to 300°C (wet)]

A nominal solid volume fraction ($v_{f,s}$) of 0.14 was developed in Section 2.1. This value was doubled ($v_{f,s}$ = 0.28) for the sensitivity calculations; the corresponding solid mass fraction ($m_{f,s}$) increases from 0.28 to 0.48. The development of the nominal property set for the temperature range from 40 to 300°C considering the specific heat increase due to boiling was discussed in Section 3.3.3; the nominal property set was given in Table 3. The property set for the increased solid volume fraction is given in Table 5; the nominal set is also given for comparison. Increasing the solid volume fraction by a factor of 2 significantly increases the thermal conductivity due to the increase in the heat transport area available after dryout. The deposit density after dryout is a linear function of the solid volume fraction since the steam mass is insignificant compared to that of the solid. The contribution to the deposit specific heat due to boiling [ΔC_p, eqn. (14)] decreases from 24.8 to 10.5 J/g/K; note that the decrease on a per unit volume of deposit basis [e.g. $(\Delta C_p)\cdot(\rho_{eff})$] is proportional to the water volume fraction prior to dryout, which decreases by 16% (from 0.86 to 0.72). The contribution to the deposit specific heat due to the solid increases with the solid volume fraction.

3.6.2 Sensitivity of Surface Temperature Values

The calculation of the time required for the surface temperature to increase from 40 to 300°C with the small pore model was discussed in Section 3.5.1; the results obtained with the nominal property set were summarized in Table 4. The same calculation was repeated using the increased solid volume fraction property data set given in Table 5. The results are given in Table 6 along with those obtained with the nominal property set for comparison. The time for the surface to reach 300°C is increased significantly due to the increased effective deposit thermal conductivity. For the best-estimate cases, the increase is sufficient that ignition would not be predicted even for a deflagration occurring 30 days after a loss of the purge gas system. For the upper-bound cases, the increase is insufficient to preclude a surface temperature above 300°C even at the LFL (Case UB 15), although in this case the surface would be predicted to stay below 300°C until after the peak gas pressure had been reached. Thus, increasing the solid volume fraction of the deposit to account for the presence of KTPB reduces the calculated surface temperatures, but not by enough to change the basic conclusions of this analysis.

3.6.3 Sensitivity of Temperature Profiles

The calculation of the temperature profiles through the deposit for Cases BE 12 and UB 19a, the most severe of the best-estimate and upper-bound cases, was discussed in Section 3.5.1; the results obtained with the nominal property set were illustrated in Figures 4 and 5. The same calculation was repeated using the increased solid volume fraction property data set given in Table 5. The results are illustrated in Figures 6 and 7 for times approximately midway through and at the end of the deflagration along with those obtained with the nominal property set for comparison. As can be seen in the figures, the increased thermal conductivity and decreased specific heat associated with the increased solid volume fraction property set result in a decreased temperature near the surface and an increased temperature deeper into the deposit. For the best-estimate case, the increased solid volume fraction results show that even the surface would stay below 300°C (as discussed above) so that the calculated thermal response of the deposit is less severe with respect to combustion. For the upper-bound case, the depth to which the deposit temperature exceeds 300°C is increased by less than 0.1 mm. Thus, increasing the solid volume fraction of the deposit to account for the presence of KTPB can either increase or decrease the calculated depth to which the deposit temperature would exceed 300°C, but not by a degree sufficient to change the conclusions of this analysis.

4.0 EFFECT ON GAS PRESSURES

The thermal analyses presented in Section 3 demonstrated that the deposit surface temperature would only exceed the minimum ignition temperature (300°C) if the pore size is very small. Even in this case, the deposit surface temperature would not exceed 300°C prior to reaching the peak pressure for any of the best-estimate cases, and would only exceed this limit during the burn if the deflagration occurred long after the N_2 purge gas system was lost (> 12 days). For the upper-bound cases, the surface temperature of a deposit with small pores would exceed 300°C for the entire range of gas compositions (LFL to stoichiometric).

As shown in Section 3.5.1, even with a stoichiometric mixture of combustible gas and air (Case UB 19a), no more than a 0.4 mm layer of a deposit could be heated above the minimum ignition temperature for a solids fire (300°C) as a result of a deflagration in an ITP waste tank. Walker (1990) gives a total energy release of $8x10^4$ kcal for complete combustion of a 1 cm thick deposit layer which coats a 10 cm width of the primary liner inner surface and cooling coil outer surfaces; as discussed in Section 2.3, this should be considered an upper bound value. The maximum energy release for complete combustion of a 0.4 mm layer of this deposit would therefore be 3,200 kcal [(80,000 kcal)·(0.04 cm)/(1 cm) = 3,200 kcal]. The volumetric energy release for a deflagration of a combustible gas with a hydrogen to benzene mole ratio of 40/60 in stoichiometric proportions with air at 40°C containing 6.6% water vapor (e.g. Case UB 19a) is 0.74 kcal/l [calculated using method presented in Thomas (1993)]. The total internal volume for a Type IIIA waste tank is approximately $5.2x10^6$ liters, so the total energy release from a deflagration of this mixture in a tank with a 1/10 fill level would be $3.5x10^6$ kcal. The total energy release associated with the deflagration would therefore be increased by less than 0.1% from the combustion of a 0.4 mm thick deposit layer.

The conservatisms in the DPAC calculation of the deflagration pressure, discussed in Thomas and Hensel (1993a), introduce a sufficient margin that a 0.1% increase in the total energy release need not be considered. Furthermore, it should be realized that even this small contribution is an overestimate because, as discussed in Section 2.2, the solid combustion process would consume oxygen from the environment. No oxygen would be available behind the flame front in a stoichiometric mixture deflagration and any oxygen consumed by a solids fire ahead of the flame front would decrease the energy released by the deflagration.

The maximum energy release from a solids fire with the best-estimate mixtures is even less than discussed above. Furthermore, all of the best-estimate mixtures are very fuel rich (Thomas and Hensel 1993a) and hence any oxygen consumption via a solids fire would decrease the energy available from gas combustion.

5.0 CONCLUSIONS

Solid deposits would be expected to have a very high water content (≈ 72 wt.%) based on the conditions which would exist inside the waste tank following a loss of the purge gas system. This water content precludes deposit combustion prior to drying via energy deposition at the surface and conduction into the deposit. Based on consideration of the magnitude and rate of energy release by solids combustion, it was concluded that ignition must be achieved prior to the time at which the peak gas pressure from the deflagration is reached in order to increase the peak gas pressure.

Thermal analyses were performed using a one-dimensional conduction model, radiative heat flux values calculated with the Deflagration Pressure Analysis Code (DPAC), and effective deposit properties calculated from the component properties. The solid portion of the deposit was assumed to be entirely $NaNO_3$ since this would be the major component in deposits most capable of sustained combustion. The thermal analyses demonstrated that the deposit surface temperature would only exceed the minimum ignition temperature (300°C) if the pore size is very small. Even in this case, the deposit surface temperature would not exceed 300°C prior to reaching the peak pressure for any of the best-estimate cases, and would only exceed 300°C during the remainder of the burn time if the deflagration occurred long after the loss of the purge gas system (> 12 days). The surface temperature of a deposit with small pores would exceed 300°C for the entire range of upper-bound cases (LFL to stoichiometric). Even with a stoichiometric mixture of combustibles with air, no more than a 0.4 mm deposit layer could be heated above 300°C as a result of an ITP waste tank deflagration.

The major uncertainty in the thermal analyses is the composition of the solid portion of the deposit. To examine the sensitivity of the results to this uncertainty, it was assumed that the solid was entirely KTPB (rather than $NaNO_3$); this change had only a minor effect on the results and did not alter the conclusions of the analysis.

The maximum energy release for complete combustion of a 0.4 mm deposit layer would be 3,200 kcal, which is less than 0.1% of the energy released from deflagration of the corresponding gas mixture. The conservatisms in the deflagration pressure calculation introduce sufficient margin that this increase need not be considered. Furthermore, even this small increase is an overestimate because the solid combustion process would consume oxygen thus decreasing the energy released by the deflagration.

6.0 REFERENCES

Allison, D.K. and S. Chow (1993) Deflagration Analysis of the ITP Facility Utilizing the MELCOR/SR Code, WSRC-RP-93-599, Savannah River Site, Aiken, SC, April 1993.

Arnott, S. and S.C. Abrahams (1958) "The Lattice Constants of the Alkali Salts of Tetraphenyl Boron," Acta Cryst., 11: 449-50.

Carslaw, H.S. and J.C. Yeager (1959) Conduction of Heat in Solids, 2nd Edition, University Press, Oxford.

Fox, R.W. and A. T. McDonald (1978) Introduction to Fluid Mechanics, 2nd Edition, John Wiley & Sons, New York, NY.

Hensel, S.J. (1993) Description and Benchmarking of the Deflagration Pressure Analysis Code (DPAC), WSRC-RD-93-008, Savannah River Site, Aiken, SC, April 1993.

Hovis, G.L. and J.F. McGlynn (1993) Solid KTPB Thermal Conductivity Experiments, WSRC-TR-93-092, Rev.1, Savannah River Site, Aiken, SC, March 1993.

Incropera, F.P. and D.P. DeWitt (1981) Fundamentals of Heat Transfer, John Wiley & Sons, New York, NY.

Morin, J.P. (1993) "Analysis of ITP Waste Tank Deflagration Conditions," WMER-ENG-93-0036, Interoffice Memorandum, Savannah River Site, Aiken, SC, 6/22/93.

Thomas, J.K. (1993) Combustion, Flame Front Propagation, and Radiative Heat Transfer Models for Deflagrations, WSRC-RD-93-007, Savannah River Site, Aiken, SC, April 1993.

Thomas, J.K. and S.J. Hensel (1993a) Pressure Resulting from an ITP Waste Tank Deflagration, WSRC-RP-93-542, Savannah River Site, Aiken, SC, April 1993.

Thomas, J.K. and S.J. Hensel (1993b) "Thermodynamic Considerations Associated with Tank Deflagrations," SRTC/NRTSC Task Plan No. 93-009-1, Savannah River Site, Aiken, SC, 1/26/93.

Touloukian, Y.S. and E.H. Buyco (1970) Thermophysical Properties of Matter, Vol. 5 - Specific Heat, Nonmetallic Solids, IFI/Plenum, New York, NY.

Touloukian, Y.S., R.W. Powell, C.Y. Ho and P.G. Klemens (1970) Thermophysical Properties of Matter, Vol. 2 - Thermal Conductivity, Nonmetallic Solids, IFI/Plenum, New York, NY.

Walker, D.D. (1989) Combustibility of Tetraphenylborate Solids, WSRC-RP-89-261, Savannah River Site, Aiken, SC, May 1989.

Walker, D.D. (1990) "Pressure Produced from Vapor and Solid Deflagration in a Waste Tank," IWT-LWP-90-0180, Interoffice Memorandum, Savannah River Site, Aiken, SC, 10/23/90.

Walker, D.D. (1993) Combustibility of ITP Slurries, WSRC-RP-93-868, Savannah River Site, Aiken, SC, June 1993.

Walker, D.D. and M.A. Schmitz (1984) Technical Data Summary - In-Tank Precipitation Processing of Soluble High Level Waste, DPSTD-84-103, Savannah River Site, Aiken, SC, May 1984.

Weast, R.C. and M.J. Astle (1982) CRC Handbook of Chemistry and Physics, 63rd Edition, CRC Press Inc., Boca Raton, FA, p. B-124.

Table 1 Summary of Input Data for Bounding Deflagration Cases.

Case Description (Tank 48, 1/10 Fill Level, Normal Generation Rates)	Case No. [a]	Avg. Radiative Heat Flux (W/cm^2) [b]		Peak Pres. (psig)	Time to Peak Pres. (sec) [c]	Burn Time (sec)
		to peak pres.	entire burn			
Best-Estimate Mixtures						
3 days after loss of purge	BE 7	0.25	0.29	≈ 13	17	23
12 days after loss of purge	BE 9	3.9	4.1	≈ 13	5.2	17
30 days after loss of purge	BE 12	5.6	5.6	≈ 13	4.6	17
Upper-Bound Mixtures [b]						
Lower Flam. Limit (LFL)	UB 15	7.1	5.5	≈ 13	9.8	38
1/2 between LFL & Stoich.	UB 17	21	17	13.4	3.0	12
Stoichiometric	UB 19a	34	32	21.3	3.8	6.7

Notes: [a] Case nos. from Thomas and Hensel (1993a) [BE = best-estimate, UB = upper-bound].
[b] Average radiative flux on cooling coil tubes, values for primary liner are 10 - 15% lower.
[c] For cases where the peak pressure was calculated to occur at the end of the burn due to autoignition , this is the time to reach the pressure required to open the vents (13 psig).

Table 2 Gas Compositions (Thomas and Hensel 1993a)

Case No.	Gas Mixture Compositions (%)					
	H_2	C_6H_6	comb.	O_2	N_2	H_2O
BE 7	0.18	0.28	0.46	6.62	85.64	7.28
BE 9	0.64	1.01	1.65	7.53	83.55	7.28
BE 12	1.44	2.27	3.71	9.10	79.91	7.28
UB 15	0.90	1.34	2.24	20.53	77.23	0.00
UB 17	1.30	1.96	3.26	20.32	76.42	0.00
UB 19a	1.60	2.40	4.00	18.80	70.65	6.55

Table 3 Summary of Solid Deposit Thermal Property Values.

	Wt. Frac. (w_f)	Vol. Frac. (v_f)	Spec. Heat (J/g/K)	Conductivity (W/m/K)	Density (gm/cm^3)
100°C (wet)					
$NaNO_3$	0.28	0.14	1.2	0.57	2.3
H_2O	0.72	0.86	4.2	0.68	0.96
Effective	1.00	1.00	3.4	0.66	1.2
100 to 300°C (dry)					
$NaNO_3$	1	0.14	1.4	0.57	2.3
H_2O [a]	0	0.86	-----	0.032	-----
Effective	1	1.00	1.4	0.087	0.32
40 to 300°C (wet)					
$NaNO_3$	1	0.14	1.4	0.57	2.3
H_2O [a]	0	0.86	-----	0.032	-----
Effective	1	1.00	26.2 [b]	0.087	0.32

Notes: [a] Heat capacity of steam neglected (e.g. steam mass fraction taken to be zero).
[b] Includes contribution of 24.8 J/g/K to account for the energy required to heat the water from 40 to 100°C and then boil it [eqn.(14)]. A value of 25 J/g/K was employed in the calculations.

Table 4 Results of Thermal Analyses.

Case No. & Type [a]	Time (sec) [a]	Avg. Radiative Flux [a] (W/cm^2)	Time (sec) Required to Cover Given Temperature Range				
			Sml. Pore Model (Charcoal)		Large Pore Model (Sponge)		
			40 to 100°C [b]	40 to 300 °C [c]	boil water in 1st cell [d]	100 to 300°C [e]	40 to 300 °C [f]
BE 7, peak	17	0.25	>> 17	------	>> 17	------	------
BE 7, burn	23	0.29	>> 23	------	>> 23	------	------
BE 9, peak	5.2	3.9	5.0	24	58	0.81	64
BE 9, burn	17	4.1	4.5	22	55	0.73	60
BE 12, peak	4.6	5.6	2.4	12	40	0.39	43
BE 12, burn	17	5.6	2.4	12	40	0.39	43
UB 15, peak	9.8	7.1	1.5	7.3	32	0.24	34
UB 15, burn	38	5.5	2.5	12	41	0.40	44
UB 17, peak	3.0	21	0.17	0.84	10.7	0.03	11
UB 17, burn	12	17	0.26	1.2	13.3	0.04	14
UB 19a, peak	3.8	34	0.07	0.32	6.6	0.01	6.7
UB 19a, burn	6.7	32	0.07	0.36	7.1	0.01	7.2

Notes: [a] 'peak' refers to the time required to reach the peak gas pressure and avg. radiative heat flux over this time, while 'burn' refers to the entire burn time and avg. heat flux over this time.
[b] Calculated with eqn.(7) and 1st set of property data in Table 3.
[c] Calculated with eqn.(7) and 3rd set of property data in Table 3.
[d] Calculated with eqn.(14).
[e] Calculated with eqn.(7) and 2nd set of property data in Table 3.
[f] Sum of times required to increase temperature from 40 to 100°C (fine pore model), boil water in 1st cell, and increase temperature from 100 to 300°C (coarse pore model).

Table 5 Effect of Solid Volume Fraction on Deposit Properties (40 to 300°C, wet).

	Wt. Frac. (w_f)	Vol. Frac. (v_f)	Spec. Heat (J/g/K)	Conductivity (W/m/K)	Density (gm/cm^3)
Nominal $v_{f,s}$					
$NaNO_3$	1	0.14	1.4	0.57	2.3
H_2O	0	0.86	-----	0.032	-----
Effective	1	1.00	26.2	0.087	0.32
Twice Nominal $v_{f,s}$					
$NaNO_3$	1	0.28	1.4	0.57	2.3
H_2O	0	0.72	-----	0.032	-----
Effective	1	1.00	11.9	0.15	0.64

Table 6 Effect of Solid Volume Fraction on Time to Reach 300°C.

Case No. & Type	Time (sec)	Avg. Radiative Flux (W/cm^2)	Time (sec) to Increase Surface Temperature from 40 to 300°C [b]	
			Nominal Solid Volume Fraction	Twice Nominal Solid Vol. Fraction
BE 7, peak	17	0.25	>> 17	>> 17
BE 7, burn	23	0.29	>> 23	>> 23
BE 9, peak	5.2	3.9	24	40
BE 9, burn	17	4.1	22	36
BE 12, peak	4.6	5.6	12	19
BE 12, burn	17	5.6	12	19
UB 15, peak	9.8	7.1	7.3	12
UB 15, burn	38	5.5	12	20
UB 17, peak	3.0	21	0.84	1.4
UB 17, burn	12	17	1.2	2.1
UB 19a, peak	3.8	34	0.32	0.52
UB 19a, burn	6.7	32	0.36	0.59

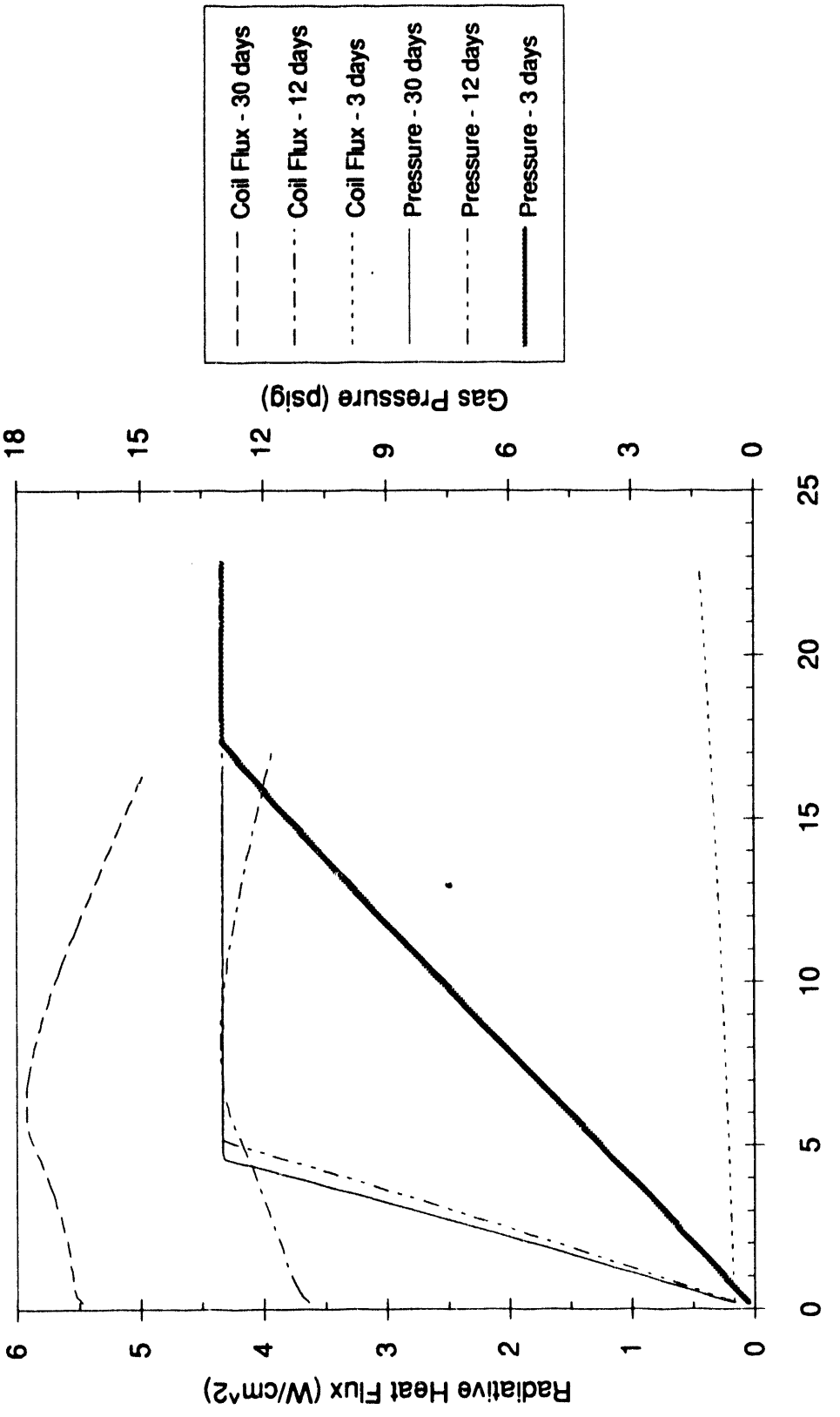

Figure 1 Heat Flux and Pressure for Best-Estimate Cases.

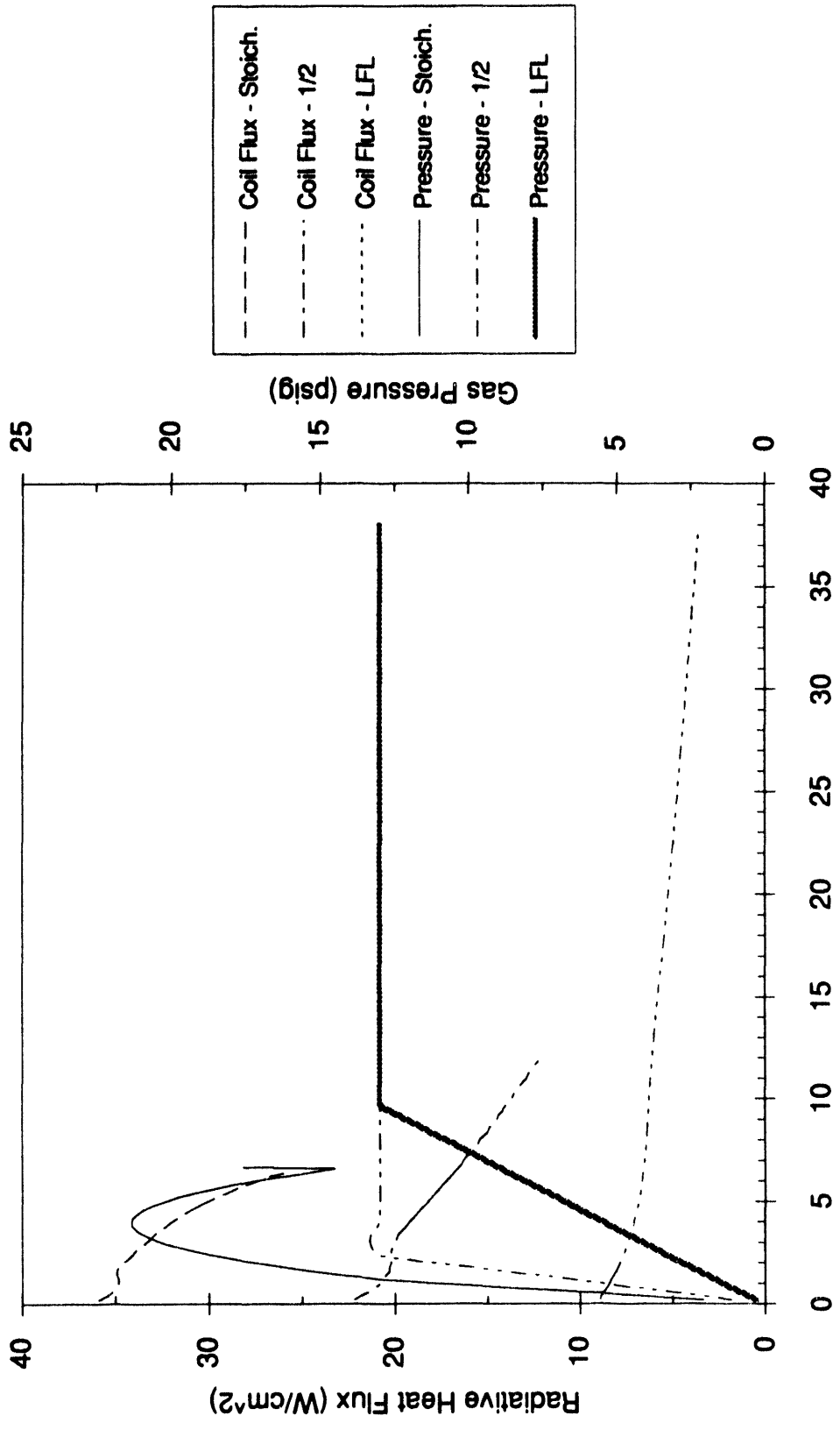

Figure 2 Heat Flux and Pressure for Upper-Bound Cases.

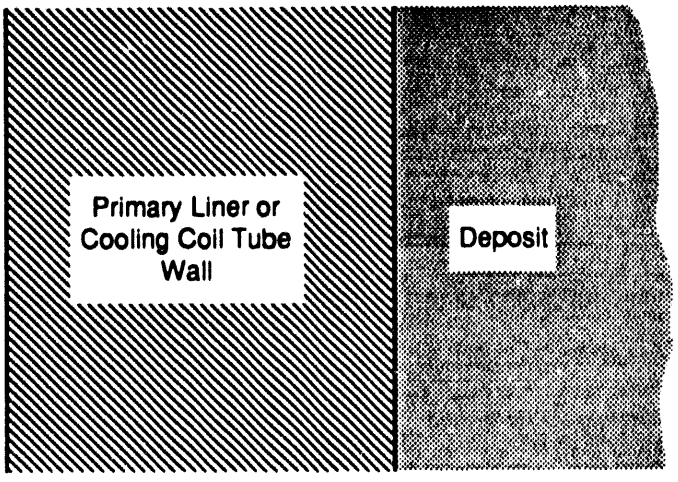

Figure 3a Small Pore Model Schematic.

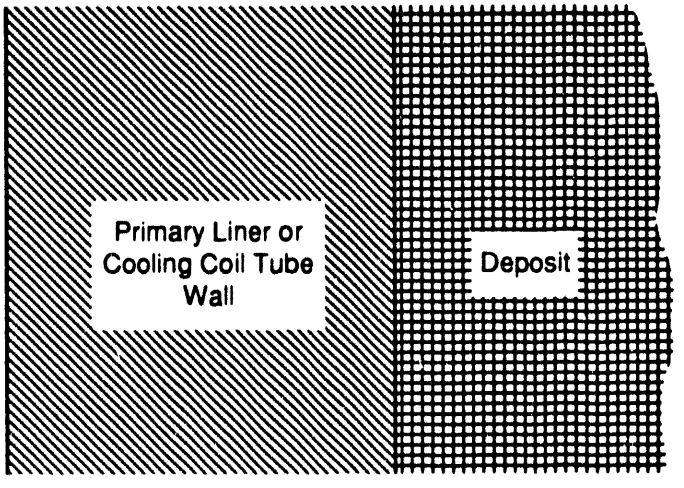

Figure 3b Large Pore Model Schematic.

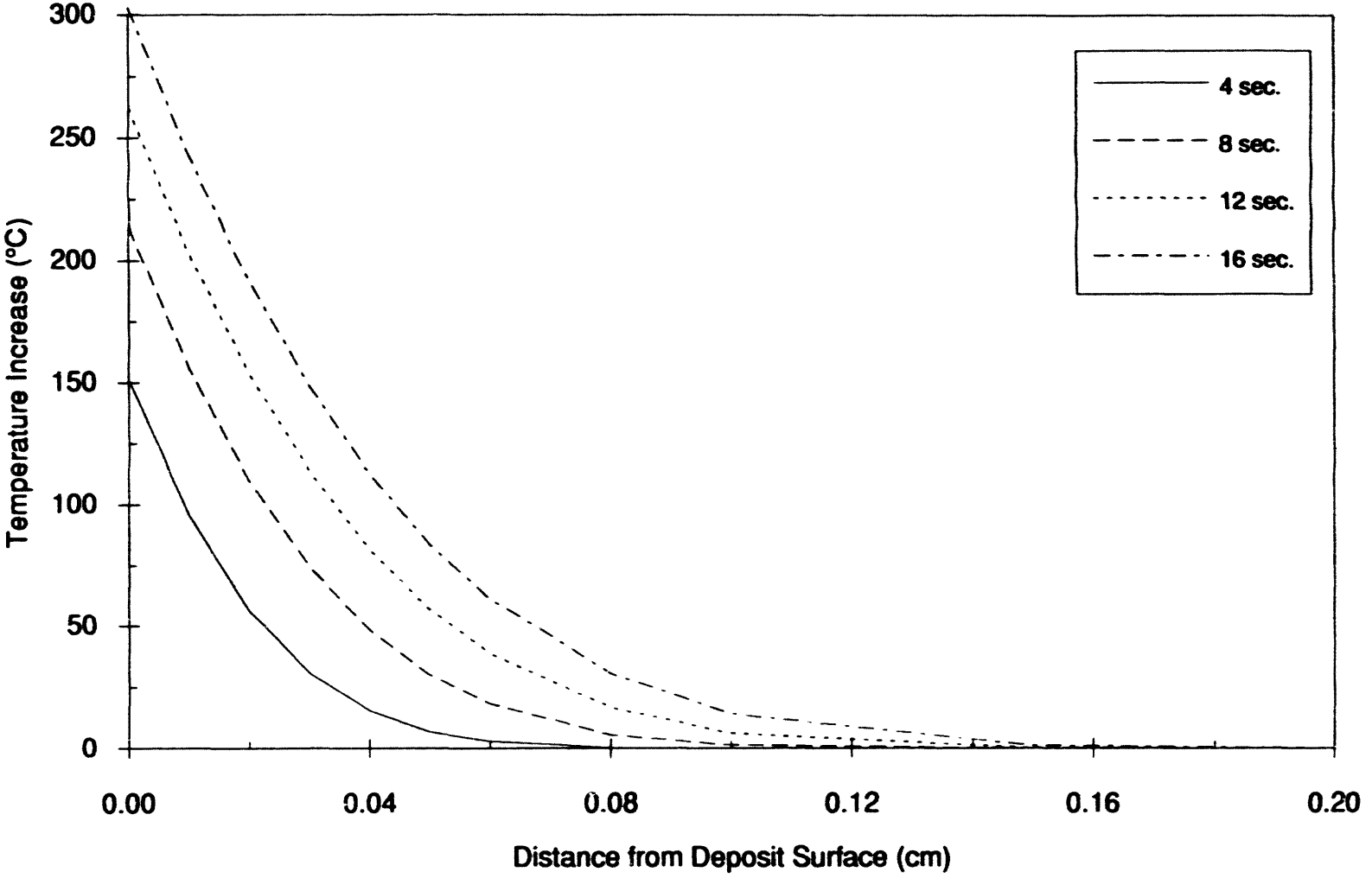

Figure 4 Temperature Profiles for Best-Estimate Case 12 (30 days).

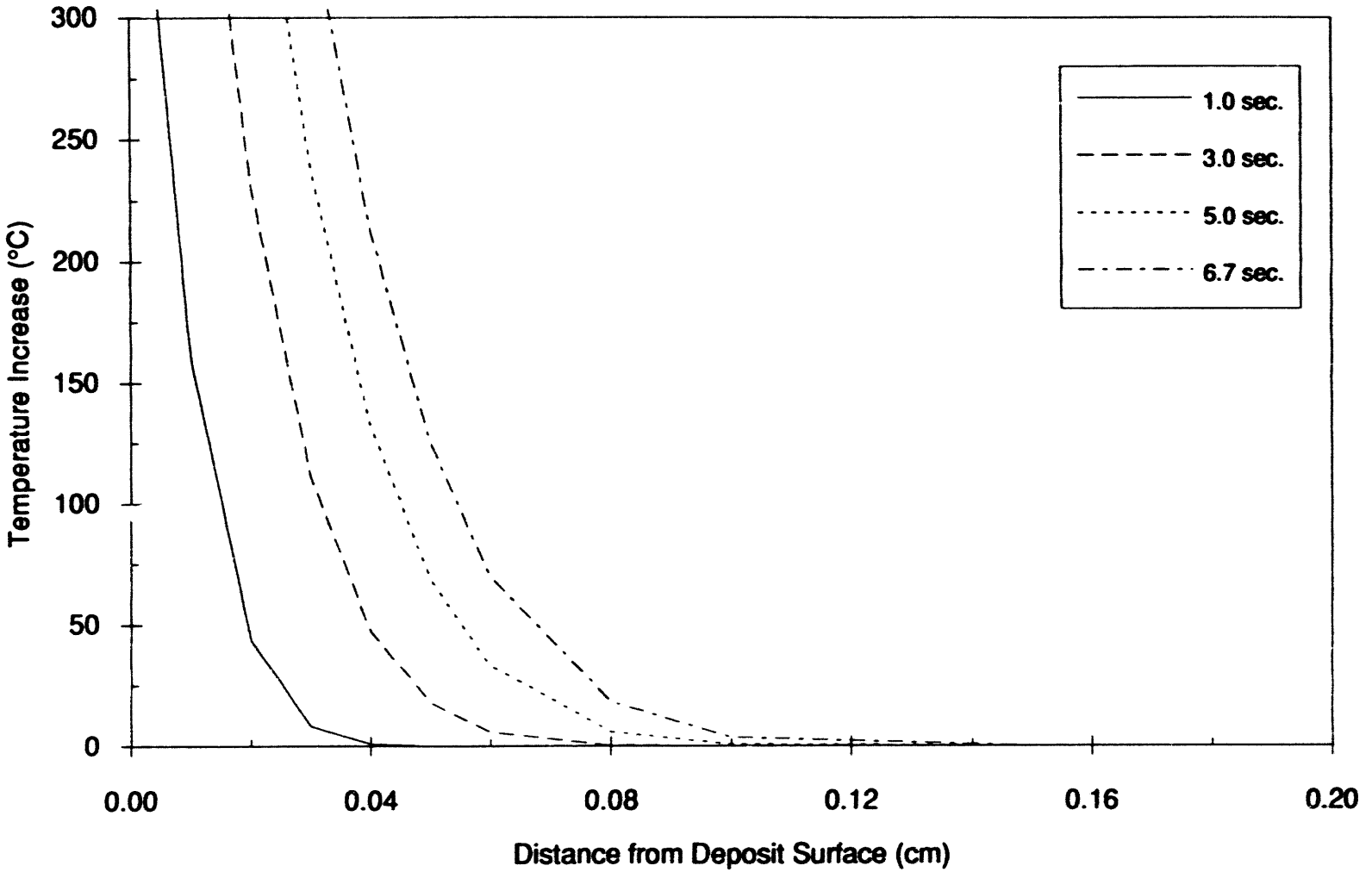

Figure 5 Temperature Profiles for Upper-Bound Case 19a (stoichiometric).

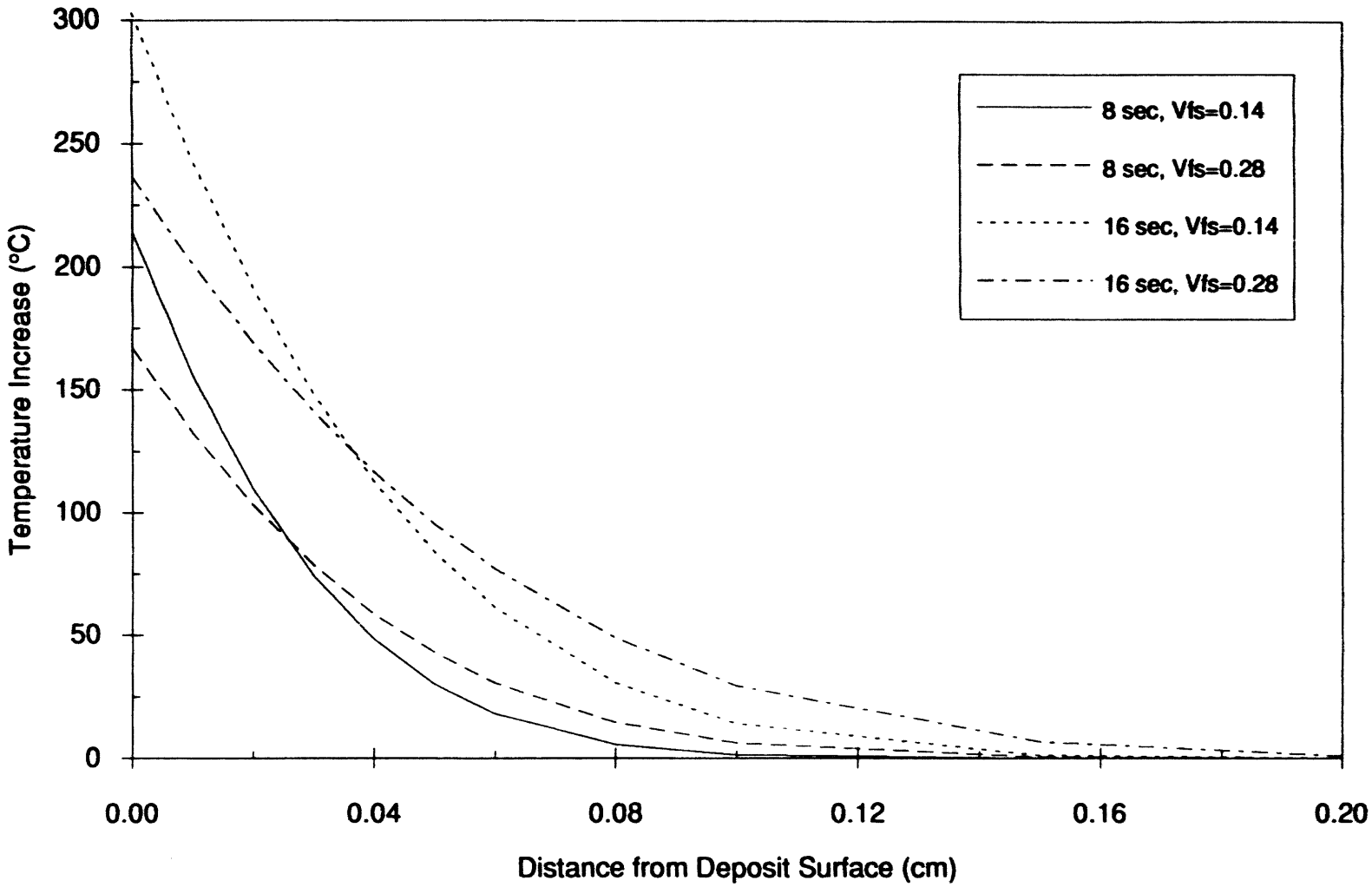

Figure 6 Effect of Solid Volume Fraction on Temperature Profiles for Case BE12.

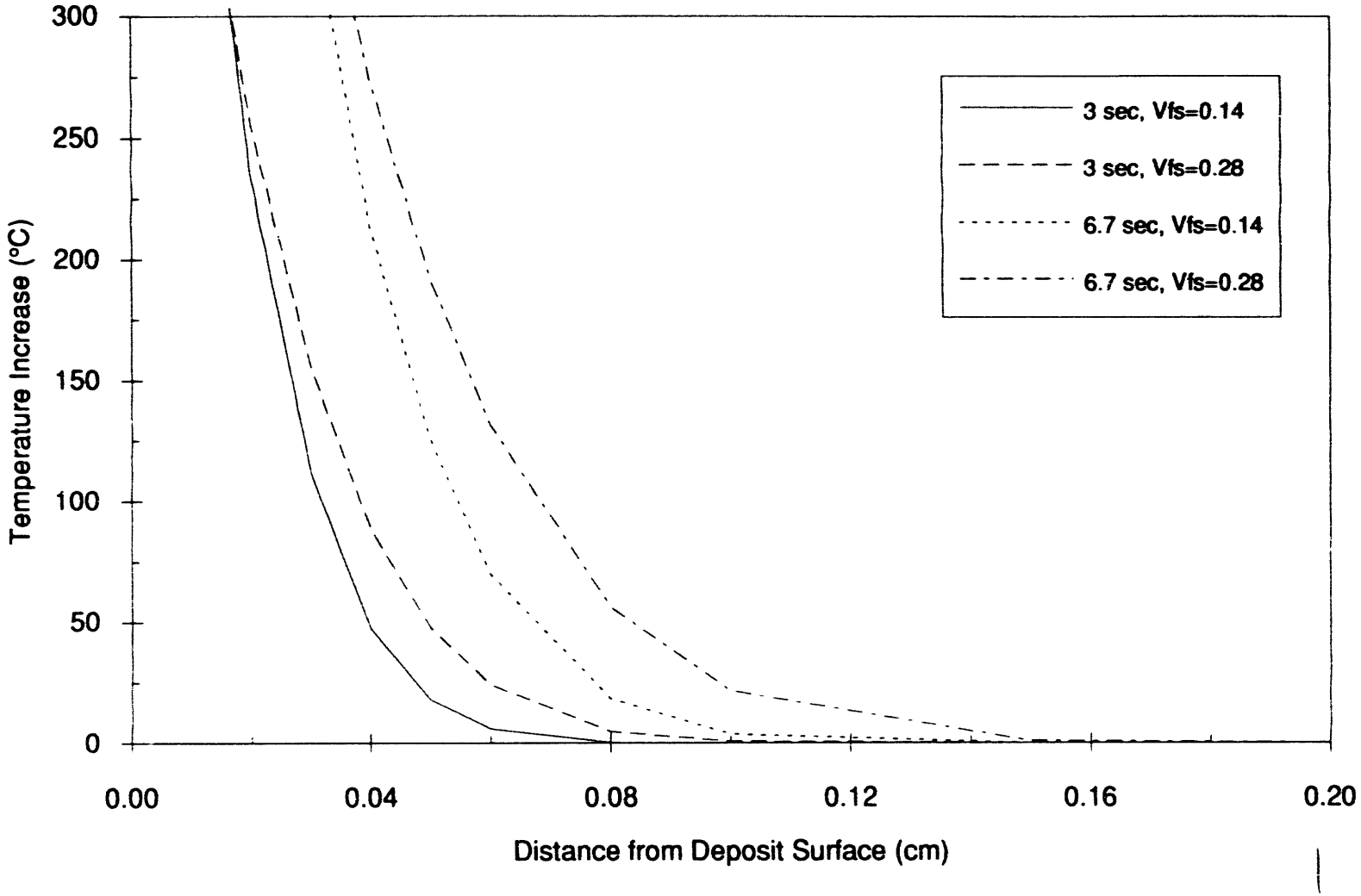

Figure 7 Effect of Solid Volume Fraction on Temperature Profiles for Case UB19a.

Appendix A - Unit Cell Description and Effective Deposit Thermal Conductivity

The effective thermal conductivity of the deposit is dependent upon the geometric arrangement of the solid and liquid phases. For the purposes of this evaluation, the deposit is assumed to be a square grid of $NaNO_3$ (e.g. cubes of solid $NaNO_3$ containing cubical pores filled with H_2O). A 2D schematic of a unit cell comprising the grid is shown in Figure A1. The solid wall thickness can be related to the liquid volume fraction as shown below:

$$v_{f,l} = \frac{V_l}{V_c} = \left(\frac{L - x}{L}\right)^3 \qquad \text{(A1)}$$

where: $v_{f,l}$ = Liquid volume fraction,
V_l = Liquid volume,
V_c = Cell volume,
L = Cell edge length, and
x = Solid wall thickness.

The cell edge length is unity since this is a unit cell (e.g. 'x' is a fractional length). The solid wall thickness can therefore be calculated as:

$$v_{f,l} = \left(\frac{1 - x}{1}\right)^3 = (1 - x)^3$$

$$x = 1 - (v_{f,l})^{1/3} \qquad \text{(A2)}$$

If the cell edge length is not taken to be unity ($L \neq 1$), then from eqn.(A1) the solid wall thickness may be expressed in terms of the liquid volume fraction and liquid layer thickness (w) as shown below:

$$v_{f,l} = \frac{V_l}{V_c} = \left(\frac{L - x}{L}\right)^3 = \left(\frac{w}{w + x}\right)^3$$

$$(v_{f,l})^{-1/3} = 1 + \frac{x}{w}$$

$$x = w\left[(v_{f,l})^{-1/3} - 1\right] \qquad \text{(A3)}$$

The effective thermal conductivity of the unit cell can be calculated using the electrical resistance analog method (Incropera and DeWitt 1981), as shown below:

$$k_{eff} = \frac{1}{R_{eq}} \qquad \text{(A4)}$$

$$R_{eq} = \frac{\Delta x}{k A} \tag{A5}$$

where: k_{eff} = Effective cell thermal conductivity,
R_{eq} = Equivalent electrical resistance,
ΔT = Temperature drop across region,
Δx = Distance over which temperature drop occurs, and
A = Area available for heat transfer.

The equivalent resistance for region A (Fig.A1) is that for the 2 solid regions (cell side walls and cell top/bottom walls) and the single liquid region all in parallel. The equivalent resistance for the unit cell is the resistance for region A in series with that for the cell front/back walls. These individual resistances are given below:

$$R_{s,s} = \frac{L - x}{k_s (L - x) x} = \frac{1}{k_s x} \tag{A6}$$

$$R_{s,tb} = \frac{L - x}{k_s L x} = \frac{1 - x}{k_s x} \tag{A7}$$

$$R_l = \frac{L - x}{k_l (L - x)^2} = \frac{1}{k_l (1 - x)} \tag{A8}$$

$$R_{s,fb} = \frac{x}{k_s L^2} = \frac{x}{k_s} \tag{A9}$$

where: $R_{s,s}$ = Equivalent resistance for solid side cell walls
$R_{s,tb}$ = Equivalent resistance for solid top and bottom cell walls,
R_l = Equivalent resistance for liquid portion of cell, and
$R_{s,fb}$ = Equivalent resistance for solid front and back cell walls,
k_s = Thermal conductivity of material comprising cell walls (solid), and
k_l = Thermal conductivity of material in cubical pore (liquid).

The equivalent resistance for region A (R_A) is:

$$R_A = \frac{1}{\frac{1}{R_{s,s}} + \frac{1}{R_{s,tb}} + \frac{1}{R_l}} = \frac{1}{k_s x + \frac{k_s x}{1 - x} + k_l (1 - x)}$$

$$R_A = \frac{1 - x}{k_s x (2 - x) + k_l (1 - x)^2} \tag{A10}$$

The equivalent resistance for the unit cell can then be written as:

$$R_{eq} = R_{s,fb} + R_A = \frac{x}{k_s} + \frac{1 - x}{k_s x (2 - x) + k_l (1 - x)^2} \tag{A11}$$

The effective thermal conductivity is the inverse of the equivalent resistance (A11), as shown below:

$$k_{eff} = \frac{k_s^2 x(2-x) + k_l k_s (1-x)^2}{k_s x^2 (2-x) + k_l x (1-x)^2 + k_s (1-x)}$$

which can also be written as:

$$k_{eff} = \frac{k_s \left(\frac{2-x}{1-x}\right) + k_l \left(\frac{1-x}{x}\right)}{x\left(\frac{2-x}{1-x}\right) + \frac{k_l}{k_s}(1-x) + \frac{1}{x}} \qquad \text{(A12)}$$

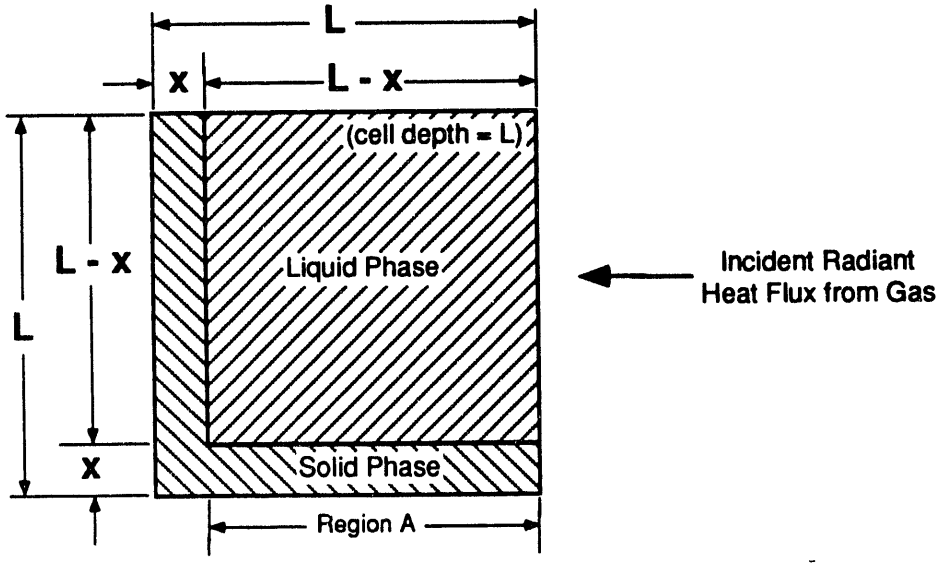

Figure A1 Unit Cell Schematic.

Appendix B - Convective Heat Transfer Contribution

This appendix presents an evaluation of the contribution from convective heat transfer to the total heat flux incident on surfaces inside a waste tank during a deflagration. The heat fluxes used in the body of this report are those due to radiative heat transfer as calculated with the Deflagration Pressure Analysis Code (DPAC); it was assumed that convection would make only a minor contribution. The convective heat flux to the cooling coil tubes is evaluated since it would be larger than that to the primary liner inner surface.

The convective heat flux to the surface of a tube immersed in flowing gas can be calculated as:

$$q_c = h\,\Delta T \tag{B1}$$

$$h = \frac{Nu_D\,k}{D} \tag{B2}$$

where: q_c = Convective heat flux,
h = Convective heat transfer coefficient,
ΔT = Temperature difference between the gas and tube surface,
Nu_D = Nusselt number for the tube,
k = Fluid thermal conductivity, and
D = Tube diameter.

The Type IIIA waste tank cooling coil tubes have an outer diameter of 2.375". The Nusselt number for a tube in flowing gas can be calculated with the following correlation (Incropera and DeWitt 1981):

$$Nu_D = \left[(0.4)Re_D^{1/2} + (0.06)Re_D^{2/3}\right](Pr^{0.4})\left(\frac{\mu_b}{\mu_s}\right)^{1/4} \tag{B3}$$

for: $0.67 < Pr < 300$,
$10 < ReD < 105$, and
$0.25 < \mu_b/\mu_s < 5.2$.

$$Re_D = \frac{\rho\,V\,D}{\mu} \tag{B4}$$

where: Re_D = Reynold's number,
Pr = Prandtl number,
μ = Fluid dynamic (absolute) viscosity,
ρ = Fluid density, and
V = Fluid velocity.

The 'b' and 's' subscripts on viscosity denote evaluation at the bulk gas temperature and surface temperature, respectively; all properties without subscripts are to be evaluated at the bulk gas temperature (e.g. all properties except μ_s)

The uncombusted reactant gas (e.g. the gas ahead of the flame front) would be at approximately the same temperature as the surfaces inside the waste tank and hence would not transfer heat to these surfaces. The temperature of the product gas (e.g. the gas behind the flame front) depends on the reactant gas composition. For Tank 48 at a 1/10 fill level, the product gas temperature for a stoichiometric mixture with air (Case UB19) would be approximately 2200 K while that for the LFL mixture (Case UB15) would be approximately 1300 K [Thomas and Hensel 1993 (Appendix B)]. Is noted that the product gas temperatures calculated assuming a closed vessel and adiabatic isochoric conditions are higher than those given above (Thomas 1993); these differences reflect the effects of venting, radiative heat transfer, and gas P·dV as calculated by DPAC. Heat transfer coefficients were calculated at both 1300, 1750, and 2200 K so as to span the range of interest.

The bulk gas properties were evaluated at the temperatures given above. The surface was assumed to be at 300 K. Air properties were employed for the gas mixture; this is obviously a simplification, but should not lead to significant error since nitrogen is the dominant component in both air and in the product gas for both the upper-bound and best-estimate mixtures. With the exception of the gas density, all properties were evaluated at a pressure of 1 atmosphere since they are relatively insensitive to pressure (Incropera and DeWitt 1981, Fox and McDonald 1978). The gas density was evaluated using the ideal gas law at an absolute gas pressure of 2.5 atmospheres, which bounds the peak gas pressures calculated by Thomas and Hensel (1993a) for deflagrations in the ITP waste tanks; the convective heat transfer coefficient increases with gas density so that this approach maximizes the contribution from convection. All property data were taken from Incropera and DeWitt (1981).

In addition to the gas properties, the gas velocity is also required in order to evaluate the Reynold's number. The gas in the immediate vicinity of the flame front would move at the speed of the flame front, while the gas in regions well away from the flame front would have a much lower velocity and that near the ignition location would be essentially stagnant. As discussed in Thomas (1993), the average flame front velocity would vary from approximately 2 to 4 times the burning velocity (volumetric combustion rate per

unit flame front area); Thomas and Hensel (1993a) utilized burning velocities ranging from 7 ft/s for stoichiometric mixtures in air down to 1 ft/s for the mixtures near the lower flammability limit (LFL). To calculate the Reynold's number in this evaluation, gas velocities of 1 ft/s (stoichiometric mixture at 2200 K), 0.1 ft/s (LFL mixture at 1300 K), and 0.5 ft/s (intermediate mixture at 1750 K) were employed. These values were selected based on engineering judgment and are probably slightly larger than those which would actually be applicable to the average convective heat transfer condition.

Table B1 gives the gas properties employed in this evaluation and the convective heat transfer parameters calculated with eqns. (B1) through (B4). The corresponding peak radiative heat flux values from Table 1 of the main text are also given for comparison. As shown in the table, the contribution from convection to the total heat flux is 5 to 9%.

It is emphasized that the calculated convective heat flux values are only applicable to the product gas region; conversely, radiative energy would be incident on surfaces in the reactant gas region, although the radiative heat flux would be largest near the point of ignition. It is also emphasized that the calculated convective heat flux values are only applicable to the cooling coil tubes and that those for the primary liner inner surface, which represents the bulk of the available area (Thomas 1993), would be significantly lower. Based on these considerations and the values given in Table B1, it is concluded that the contribution from convection may be neglected in calculating the thermal response of the deposits to a deflagration.

Table B1 Convective Heat Transfer Results

Parameter	Product Gas Temperature (K) [T_b]		
	1300	1750	2200
Gas Velocity (ft/s)	0.1	0.5	1
Gas viscosity at T_b (N-s/m^2) [a]	4.96E-05	6.24E-05	7.40E-05
Gas density at T_b & 1 atm. (kg/m^3)	0.268	0.199	0.158
Gas Prandtl Number at T_b [Pr]	0.719	0.684	0.655
Gas Conductivity at T_b (W/m/K)	0.082	0.117	0.160
Reynold's Number {Re_D} [b, c]	25	73	98
Nusselt Number {Nu_D} [d]	2.8	5.2	6.3
Heat Transfer Coeff. (W/m^2/K)	4	10	17
Convective Heat Flux (W/cm^2)	0.4	1.5	3.2
Radiative Heat Flux (W/cm^2) [e]	7.1	21	34
Convective/Total Flux (%)	5	7	9

Notes:
[a] All gas properties taken from Incropera and DeWitt (1981).
[b] Calculated with eqn.(B4) for a tube diameter of 2.375 inches (cooling coil tube O.D.).
[c] Calculated with gas density adjusted to an absolute pressure of 2.5 atmospheres using the ideal gas law (e.g. 2.5 times the given value). All other gas properties were assumed to be independent of pressure and were evaluated at a pressure of 1 atmosphere.
[d] Calculated with eqn.(B3) for a surface temp. and viscosity of 300K & 1.85E-5 N·s/m^2.
[e] Taken from Table 1 of main text. The 1300 and 2200 K values correspond to the LFL and stoichiometric air mixture cases (UB15 and UB19), while the 1750 intermediate value was taken to be the average of these two.

DATE
FILMED
4/7/94
END